Viscoelastic lubrication of a submerged cylinder sliding down an incline

Oratis, A.T.; van den Berg, K.; Bertin, V.; Snoeijer, J.H.

DOI
10.1209/0295-5075/adbcd2

Publication date
2025

Document Version
Final published version

Published in
Europhysics Letters: a letters journal exploring the frontiers of physics

LETTER • OPEN ACCESS

Viscoelastic lubrication of a submerged cylinder sliding down an incline

To cite this article: A. T. Oratis *et al* 2025 *EPL* **149** 63002

A Letters Journal Exploring the Frontiers of Physics

March 2025

EPL, **149** (2025) 63002
doi: 10.1209/0295-5075/adbcd2

www.epljournal.org

Viscoelastic lubrication of a submerged cylinder sliding down an incline

A. T. Oratis[1,2(a)], K. van den Berg[1], V. Bertin[1,3] and J. H. Snoeijer[1]

[1] *Physics of Fluids Group, University of Twente - 7500 AE Enschede, The Netherlands*
[2] *Department of Chemical Engineering, Delft University of Technology - Delft 2629 HZ, The Netherlands*
[3] *Aix Marseille University, CNRS, IUSTI UMR 7343 - Marseille 13453, France*

received 11 December 2024; accepted in final form 5 March 2025
published online 10 April 2025

Abstract – Lubrication flows between two solid surfaces can be found in a variety of biological and engineering settings. In many of these systems, the lubricant exhibits viscoelastic properties, which modify the associated lubrication forces. Here, we experimentally study viscoelastic lubrication by considering the motion of a submerged cylinder sliding down an incline. We demonstrate that cylinders move faster when released in a viscoelastic Boger liquid compared to a Newtonian liquid with similar viscosity. Cylinders exhibit pure sliding motion in viscoelastic liquids, in contrast to the stick-slip motion observed in Newtonian liquids. We rationalize our results by using the second-order fluid model, which predicts a lift force on the cylinder arising from the normal-stress differences. The interplay between viscoelastic lift, viscous friction, and gravity leads to a prediction for the sliding speed, which is consistent with our experimental results for weakly viscoelastic flows. Finally, we identify a remarkable difference between the lubrication of cylindrical and spherical contacts, as the latter do not exhibit any lift for weak viscoelasticity.

Introduction. – Thin-film flows between solid surfaces arise in a variety of biological, environmental, and engineering settings. These lubrication flows facilitate the relative motion of the solid boundaries by reducing their friction, as in the case of mammalian synovial joints [1] or industrial bearings [2]. A characteristic feature of lubrication is the slenderness of the geometry, which prescribes the flow structure and induces a strong pressure within the liquid. The build-up of pressure generates forces on the boundaries, such as hydrodynamic friction and normal loads. Lubrication flows have thus been the focus of many studies, aided by analyses using long-wave expansions [3].

Considering the motion between two rigid objects with symmetric profiles, as in the case of a cylinder sliding parallel to a plane wall, the vertical lift force induced by the hydrodynamic pressure vanishes for a Newtonian viscous liquid. The pressure adopts an antisymmetric spatial profile, leading to a zero lift force [4]. The pressure antisymmetry can be broken by introducing elasticity in the solid boundary. For sufficiently soft walls, the coupling between lubrication and the elastic deformation of the wall generates a lift force on the cylinder [5–11]. The lift force leads to a larger separation with the wall and thus smaller lubrication friction. Consequently, cylinders move faster past soft walls as compared to rigid walls [12].

A lift force on the cylinder can also be generated by introducing elasticity inside the lubricant, as is the case for viscoelastic liquids. Indeed, polymers dissolved in the liquid can stretch with the flow and exert forces on the object arising from normal-stress differences [13]. For instance, when a pair of closely separated spheres sediment in a viscoelastic liquid, they get attracted to each other [14–17]. Replacing one of the spheres with a planar wall leads to a similar effect, with the sphere being attracted to the wall during its sedimentation [18–21]. Yet, when a cylinder moves parallel to a wall in a viscoelastic fluid the attraction becomes repulsive [21,22]. Why viscoelasticity causes an attraction for spheres and a repulsion for cylinders remains unclear.

In this letter, we experimentally study the effects of viscoelastic stresses on the sliding motion of a submerged

(a) E-mail: a.t.oratis@tudelft.nl (corresponding author)

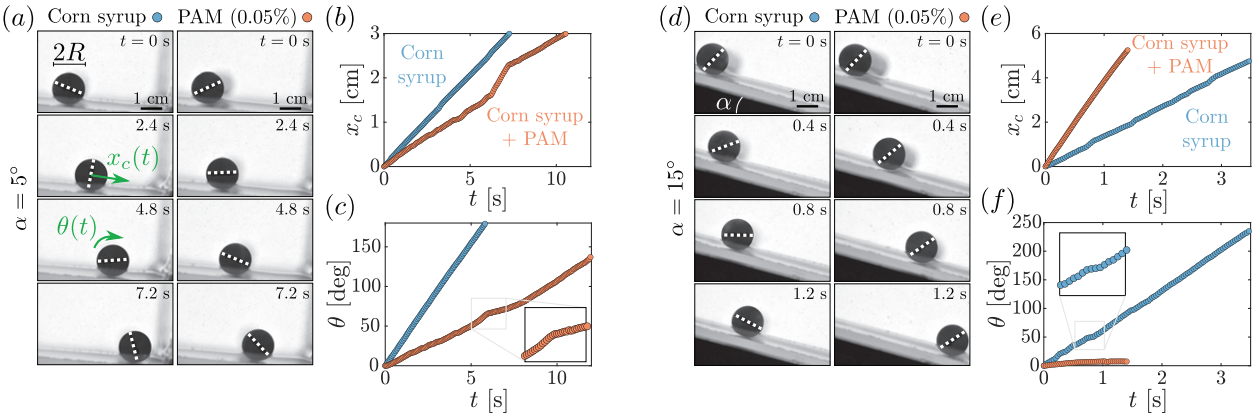

Fig. 1: (a) Experimental images of a steel cylinder with radius $R = 0.7$ cm moving down an inclined plane with inclination angle $\alpha = 5°$. The cylinder rotates as it moves in both Newtonian corn syrup solution (left) and PAM solution with $c = 0.05$ % (right). (b) The cylinder position x_c against time t shows that it moves faster in the Newtonian liquid (blue circles) than in the viscoelastic liquid (red circles), in which it exhibits stick-slip motion. (c) The cylinder rotation angle θ increases in time for both liquids. Inset: magnified plot of the rotation in the PAM solution to highlight the stick-slip motion. (d) Experimental images for the cylinder sliding at an inclination angle $\alpha = 15°$. The rotation is still apparent in the Newtonian liquid (left), but is suppressed in the viscoelastic liquid (right). (e) The evolution of x_c indicates a much faster descent when the cylinder is immersed in the viscoelastic liquid. (f) The rotation angle θ increases with time for the Newtonian liquid, whereas the increase in the viscoelastic liquid is negligible. Inset: magnification plot of rotation angle in the Newtonian liquid.

cylinder down an incline. We show that cylinders move faster in viscoelastic liquids than in Newtonian liquids, and explore to what extent these results can be interpreted using the second-order fluid model.

Experimental protocol. – To study the effects of viscoelasticity on the sliding dynamics, we use a solution comprised of water, commercially available corn syrup (Chung Jung One), and polyacrylamide (PAM $M_w = 5 \times 10^6$ g/mol, Sigma Aldrich). This combination of liquids is a common recipe used to prepare Boger fluids and probe the effects of liquid elasticity [23–27]. PAM is first dissolved into water using a magnetic stirrer for 48 hours. Five different solutions are prepared, whose PAM concentrations are $c = 0.10$, 0.25, 0.50, 0.75, and 1.00 wt.%. The concentration at which the PAM polymer chains in water begin to overlap is approximately $c^* \approx 0.5$ wt.% [28]. Therefore, our water-PAM solutions can be classified being near the transition from dilute to semi-dilute. The water-PAM solutions are then dissolved in corn syrup at a mass ratio 10:90 using a roller bank for four days. A Newtonian liquid is prepared in the same manner, without dissolving PAM into water. Each solution is measured to have the same liquid density of $\rho_\ell = 1350$ kg/m^3.

The rheology of every solution is characterized using a rheometer (MCR 502 with CP50-1, Anton Paar) in a cone-plate configuration by measuring the shear stress and first normal-stress difference (see the Supplementary Material `Supplementarymaterial.pdf` (SM)). As the imposed shear rate $\dot\gamma$ increases from 0.1 to 100 (1/s), the viscosity η of each solution remains fairly constant, such that the viscoelastic liquids can be classified as Boger fluids [23]. The viscosity increases with the amount of dissolved polymer and varies moderately between $400 \leq \eta \leq 670$ mPa·s. The degree of viscoelasticity is characterized by the first normal-stress difference coefficient $\psi_1 = N_1/\dot\gamma^2$, where N_1 is the first normal-stress difference measured by the rheometer. The resulting normal-stress difference coefficient for each solution is fitted to be $\psi_1 = \{0.5, 2.9, 7.2, 13, 13\} \times 10^{-2}$ Pa·s^2 (see the SM).

Once the liquids are prepared, they are poured in a rectangular container of dimensions 30 × 20 × 20 cm. The container is then rotated by an inclination angle α, which we vary in the range $5° \leq \alpha \leq 35°$. A cylinder is released inside the liquid and its motion recorded with a camera (Nikon D850) at a frame rate of 60 frames per second. We use aluminum, brass and steel cylinders, whose densities are $\rho = 2590$, 7660, and 7970 kg/m^3, respectively. Three different aluminum cylinders are used with radii $R = 0.6$, 1.0, and 1.5 cm, while the radii of the brass and steel cylinders are $R = 0.4$ cm and $R = 0.7$ cm, respectively. The length of each cylinder is 10 cm, much larger than the radius, such that the system can be treated having a two-dimensional geometry. In addition, we also perform experiments with three steel spheres ($\rho = 7790$ kg/m^3), whose radii are $R = 0.5$, 0.8, and 1.0 cm.

Cylinders. – The motion of the steel cylinder in the container for an inclination angle of $\alpha = 5°$ is illustrated in fig. 1(a). When released inside the Newtonian liquid (*i.e.*, corn syrup/water solution), the cylinder exhibits a motion close to pure rolling, as inferred from the orientation of the dashed line on its cross-section. Similarly, for a viscoelastic solution with PAM concentration $c = 0.05$ wt.%, the cylinder also rotates during its descent. Plotting the center of mass position along the incline x_c against time t, we observe that the cylinder moves slightly faster in the

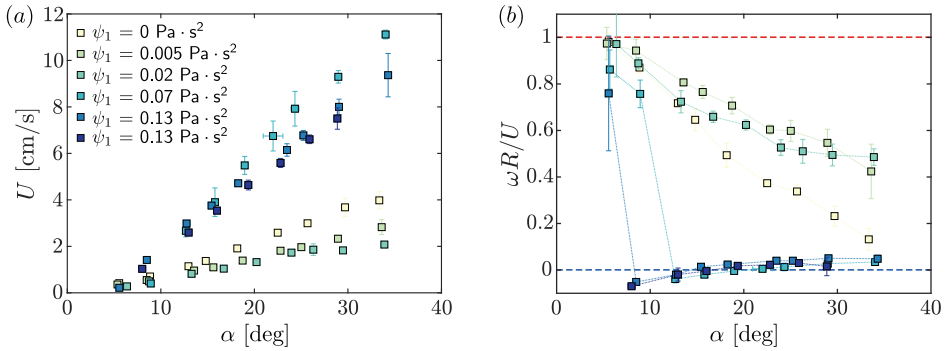

Fig. 2: (a) The velocity of the cylinder U increases with the wall inclination angle α. For large values of ψ_1 (blue squares), U increases more strongly with α compared to the Newtonian case (green squares) and low polymer concentrations (yellow squares). (b) The relative rotation velocity $\omega R/U$ against the inclination angle α. The relative rotation for the Newtonian liquid and weakly gradually decreases as the wall slope get steeper. Conversely, the strongly viscoelastic liquids undergo a sharp transition towards a rotation-free regime. The red and blue horizontal lines depict pure rotation $\omega R/U = 1$ and pure sliding $\omega R/U = 0$, respectively. Each square corresponds to the average value over five runs and the error bars represent the standard deviation.

Newtonian liquid (fig. 1(b)). The position x_c appears to be increasing continuously against time. Yet, x_c increases in a much more irregular manner in the viscoelastic liquid. The slope does not remain constant and increases at random intervals, indicative of stick-slip motion (see the supplementary movie `SuppVid1.mp4`). The same trends can be observed by examining the evolution of the cylinder rotation angle θ (fig. 1(c)). The rotation angle increases steadily for the Newtonian liquid and at a faster rate than the viscoelastic solution, whose slope changes as the cylinder alternates between rolling and sliding (fig. 1(c), inset).

Increasing the inclination angle to $\alpha = 15°$ leads to a significantly different sliding motion. While the cylinder is still rolling in the Newtonian liquid, the rotation is suppressed in the viscoelastic liquid (fig. 1(d)). The center of mass position x_c for the PAM solution no longer exhibits stick-slip and increases much faster (fig. 1(e)). This result is surprising at first glance, as the viscoelastic solution is slightly more viscous than the Newtonian liquid. Importantly, the dashed line on the cylinder cross-section retains its orientation (fig. 1(d)). As a result, the rotation angle θ barely increases for the viscoelastic liquid, such that the sliding is now rotation-free (fig. 1(f)). Conversely, the rotation angle keeps increasing for the Newtonian liquid and the cylinder undergoes a stick-slip motion (see fig. 1(e), inset and the supplementary movie `SuppVid2.mp4`). The higher sliding speed and absence of rotation in the viscoelastic liquid suggests a fundamental frictional change at the base of the cylinder.

We hypothesize that a thin liquid film is entrained beneath the cylinder. The absence of contact would indeed drastically reduce the sliding friction, in line with the absence of rotation in experiments. This phenomenology resembles the classical frictional transition in lubricated contacts. Specifically, the friction coefficient can be expressed as a function of the dimensionless parameter $\eta U/N$, where U is the sliding velocity and N the normal load per length [29,30]. For low values of $\eta U/N$, the two surfaces are in direct solid-solid contact (boundary lubrication) and the friction coefficient of order 1. For larger $\eta U/N$, a continuous film lubricates the contact (hydrodynamic lubrication) and the friction coefficient is largely reduced. An intermediate regime (mixed lubrication) separates these two cases, where there is partial contact between the surfaces. In this regime the friction decreases with velocity, which is a condition to get stick-slip motion. In our experiments, the increase of the inclination angle both increases the speed U and decreases the normal load N. The combination of these effects indeed explains why we observe a transition between a friction-dominated rolling regime at low angles, to a pure sliding regime with low friction at large angles.

To assess the effects of viscoelasticity on the sliding dynamics, we determine the cylinder velocity U and its rotational speed ω by fitting the slope of $x_c(t)$ and $\theta(t)$, respectively. The variation of the sliding velocity U and relative rotational speed $\omega R/U$, as a function of the inclination angle α, is plotted in fig. 2(a), (b). The rotational speed has been normalized, such that a value of $\omega R/U = 1$ corresponds to slip-free rolling (red dashed line in fig. 2(b)), while $\omega R/U = 0$ corresponds to pure sliding (blue dashed line in fig. 2(b)). We first focus on the Newtonian liquid (yellow squares), for which the cylinder velocity increases as the descent slope gets steeper, reaching values up to $U \approx 2$–3 cm/s. At low inclination angles, the relative rotation is close to unity, such that the cylinder exhibits a pure rolling motion without any slip (fig. 2(b)). As the inclination increases, the relative rotation decreases, moving from slip-free rolling to stick-slip dynamics. The lack of a pure sliding motion with increasing α, indicates that the dynamics never reaches the lubrication regime. There must always be some contact with the wall, suggesting a mixed lubrication, where both solid friction and hydrodynamic lubrication contribute to the sliding friction.

We now turn to the case where a small amount of polymers is dissolved in the liquid. For the viscoelastic liquids with $\psi_1 = 0.005$ and 0.029 Pa·s^2 (green squares), we again find an increase in the cylinder velocity with the inclination angle (fig. 2(a)). The cylinder velocities are slightly smaller than the Newtonian liquid, with no significant trend observed as ψ_1 increases. The relative rotation in both liquids is close to unity for small inclination angles and decreases as the inclination angle becomes steeper (fig. 2(b)). Yet, the relative rotation decreases at a slightly lower rate than the Newtonian liquid and never reaches the pure sliding regime for the range of inclination angles tested. We thus observe that for weakly viscoelastic liquids, the cylinder dynamics do not strongly deviate from those observed in the Newtonian liquid. The cylinder undergoes pure rotation or stick-slip motion with a slightly smaller velocity and higher relative rotation. There is still contact with the wall, which means that the friction remains within the mixed lubrication regime.

Increasing the amount of dissolved polymers leads to significant changes for both U and ω. For the viscoelastic liquids with $\psi_1 = 0.07$, 0.13, and 0.13 Pa·s^2 (blue squares), the cylinder velocities remain similar to the Newtonian liquid for $\alpha < 10^\circ$. Yet, beyond this inclination angle, the velocity values are much larger (fig. 2(a)). The effects of viscoelasticity are also reflected in the relative rotation. For low inclination angles, the relative rotation is high. However, unlike the Newtonian and weakly viscoelastic cases, the cylinder undergoes stick-slip motions spanning a large range in the relative rotation. The range of values of the rotation for the same value of α is also reflected by the large error bars in fig. 2(b). As the inclination angle increases, the relative rotation undergoes an abrupt transition to pure sliding. The decrease in the relative rotation is also accompanied by a significant decrease in the error bars. Interestingly, the transition even leads to a slight backspin, for which the rotation is negative $\omega < 0$. The effect of ψ_1 on both U and ω is not strong, with slightly higher velocities observed for the liquid with smaller ψ_1, suggesting a saturation of the elastic effects. The large variation in stick-slip motions at low inclination angles suggests a lower sliding friction on the cylinder, which is indicative of a mixed lubrication regime. The abrupt decrease in the relative rotation signals the transition towards the hydrodynamic lubrication regime, in which the continuous entrainment of a thin liquid film prevents the contact between cylinder and wall. Therefore, sufficiently strong normal-stress differences tend to suppress solid contact and lead to pure sliding motions.

We proceed by considering only the data of pure sliding ($\omega R/U < 0.1$) and explore cylinders of different sizes and materials, each following similar trends on the relative rotation as the one shown in fig. 2. We first test how the experimental sliding speed U compares to

$$U_{\mathrm{St}} = \frac{\Delta\rho g R^2 \sin\alpha}{\eta}. \tag{1}$$

This "Stokes" velocity scale arises from a viscogravitational balance $\Delta\rho g R^2 \sin\alpha \sim \eta U$, where $\Delta\rho = \rho - \rho_\ell$ is the density difference. Plotting the experimental velocity against U_{St}, we observe a scatter of the data (fig. 3(a)). The lack of collapse of the data is not surprising, as this velocity scale does not include the effects of lubrication. In the following we propose a mechanism that can collapse the experimentally observed velocities.

Self-sustained elastic lift. – The pure sliding regime requires a mechanism of self-sustained lift preventing solid-solid contact, which can arise from the normal-stress differences in viscoelastic liquids. To model the effects of normal stresses, we use the second-order fluid, which is the simplest constitutive relation that admits normal-stress differences. For a two-dimensional flow with velocity boundary conditions, we can utilize Tanner's theorem, which admits a Newtonian velocity field and a modified viscoelastic pressure [31,32]. Hence, by solving the velocity and pressure field of the Newtonian problem, we can obtain the viscoelastic stresses, which are required to compute the forces exerted on the cylinder. We consider the two-dimensional flow ($\hat{\mathbf{e}}_x$, $\hat{\mathbf{e}}_z$) caused by a cylinder sliding parallel to a wall at a gap distance h_0. We analyse the problem in the reference frame of the sliding cylinder, such that the wall is moving with velocity $-U$ and the flow is steady. The geometry of the liquid thickness can be approximated by a parabolic profile $h(x) = h_0[1 + x^2/(2h_0R)]$. For a sufficiently small gap h_0, the lubrication approximation, $h_0/R \ll 1$, leads to a velocity field $u(x,z) = (1/2\eta)(\mathrm{d}p_{\mathrm{N}}/\mathrm{d}x)(z^2 - zh) + U(z/h - 1)$, where we introduced the Newtonian pressure field $p_{\mathrm{N}}(x) = 2\eta U x/h(x)^2$ [4]. Combining these two expressions with the second-order fluid model, the lift force (per unit length) exerted on the cylinder can be computed analytically [32,33], which yields the following expression:

$$\mathcal{L} = \frac{\psi_1}{4}\int_{-\infty}^{\infty}\left(\frac{\partial u}{\partial z}\right)^2\bigg|_{z=h(x)}\mathrm{d}x = \frac{\pi}{2\sqrt{2}}\frac{\psi_1 U^2 R^{1/2}}{h_0^{3/2}}. \tag{2}$$

Interestingly, normal-stress differences do not generate a torque on the cylinder, nor do they modify the viscous drag [33], which is given by $\mathcal{D} = 2\sqrt{2}\pi(\eta U R^{1/2}/h_0^{1/2})$.

We now have all the expressions required to determine the steady sliding velocity of the cylinder. The lift due to the normal-stress differences $\mathcal{L}$, as given by (2), balances the weight component perpendicular to the wall,

$$\frac{\pi}{2\sqrt{2}}\frac{\psi_1 U^2 R^{1/2}}{h_0^{3/2}} = \Delta\rho g \pi R^2 \cos\alpha. \tag{3}$$

The viscous drag $\mathcal{D}$ balances the component of the weight parallel to the wall,

$$2\sqrt{2}\pi\frac{\eta U R^{1/2}}{h_0^{1/2}} = \Delta\rho g \pi R^2 \sin\alpha. \tag{4}$$

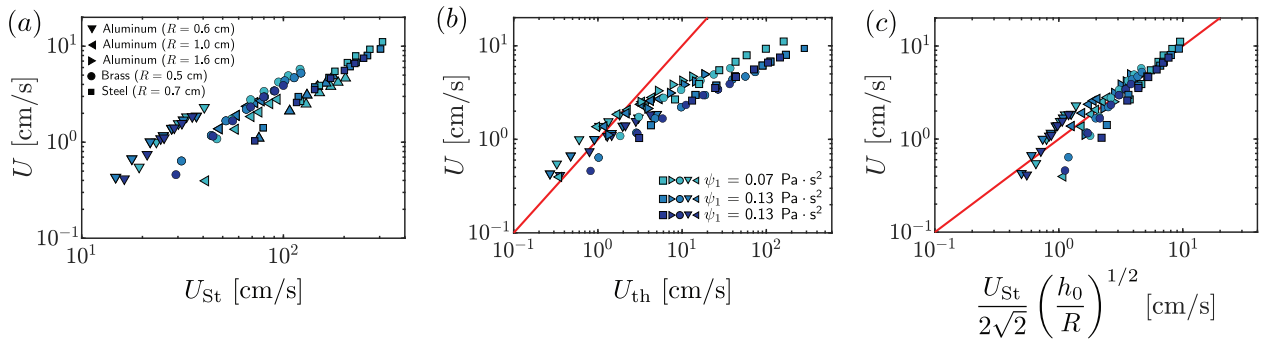

Fig. 3: Different ways of rescaling the cylinder velocity U. (a) The experimentally measured velocity U against the Stokes velocity scale $U_{\rm St} = \Delta\rho g R^2 \sin\alpha/\eta$. (b) The velocity U against $U_{\rm th}$, given by eq. (5), collapses the data. The theoretical prediction (red line) captures the smaller values of the experiments, but overestimates the velocity beyond $U \approx 2$ cm/s. (c) The lubrication velocity scaling $(U_{\rm St}/2\sqrt{2})(h_0/R)^{1/2}$ leads to a better collapse of the data using a value $h_0 = 5 \times 10^{-5}$ m.

Solving these two equations for U and h_0 yields

$$U_{\rm th} = \frac{U_{\rm St}}{64}\left(\frac{\psi_1\Delta\rho g R}{\eta^2}\right)\left(\frac{\sin^2\alpha}{\cos\alpha}\right), \qquad (5)$$

$$h_{\rm th} = \frac{R}{512}\left(\frac{\psi_1\Delta\rho g R}{\eta^2}\right)^2\left(\frac{\sin^2\alpha}{\cos\alpha}\right)^2. \qquad (6)$$

The theoretical sliding velocity has been expressed as the product of $U_{\rm St}$, defined in (1), multiplied by the geometric factor $\sin^2\alpha/\cos\alpha$ and the dimensionless viscoelastic parameter $\psi_1\Delta\rho g R/\eta^2$. The latter takes the form of a Weissenberg number $\psi_1 U_{\rm St}/(\eta R)$, with a strain rate given by $U_{\rm St}/R$.

The experimentally measured velocity against the theoretical prediction of (5) is shown in fig. 3(b). The data collapse in a much better fashion than the Stokes scaling (fig. 3(a)). In addition, the theoretical prediction (red line) captures the experimental data for low values of the velocity $U < 2$ cm/s without any adjustable parameter. For larger speeds, the prediction overestimates the cylinder velocity and the experimental data appear to have a much weaker dependence on $U_{\rm th}$. The breakdown of our model at high velocities can possibly be attributed to two main factors. First, the second-order fluid model provides a description only for weakly viscoelastic flows, *i.e.*, flows at relatively low Weissenberg numbers. For a velocity value of $U \approx 2$ cm/s, above which (5) fails to capture the experimental data, the horizontal force balance between gravity and viscosity yields a typical thickness $h_0 \sim 10^{-5}$ m. The corresponding Weissenberg number of the lubrication flow becomes ${\rm Wi} = \psi_1 U/(\eta h_0) \sim 100$, which is already very large. At such values, the dependence of the normal stresses on the shear rate might deviate from the quadratic scaling expected from the second-order fluid. Non-linear effects, such as finite extensibility or a shear-dependent normal-stress coefficient $\psi_1(\dot\gamma)$ are expected to come into play [23], which could lead to a saturation of the normal stresses. Second, the polymer solutions used are in the semi-dilute regime. As can be seen from the rheological measurement in the SM, the normal stress exhibits a dependence on $\dot\gamma$ that is slightly weaker than the quadratic fit used in the modeling.

For large cylinder velocities ($U > 2$ cm/s), the experimental data do not exhibit a strong dependence on the degree of viscoelasticity, as quantified by ψ_1 (see fig. 2(a)). We aim to describe the typical scaling of the cylinder speed in this regime, where the cylinder-wall contact is clearly still lubricated. Empirically treating h_0 as a constant thickness, the horizontal force balance (3) leads to the velocity prediction $U = (U_{\rm St}/2\sqrt{2})(h_0/R)^{1/2}$. The experimental sliding velocity agrees reasonably well with this lubrication scaling in the range $2 \leq U \leq 10$ cm/s, showing a consistency with the lubrication theory (fig. 3(c)). We empirically set the gap thickness to $h_0 = 5 \times 10^{-5}$ m such that the best agreement is obtained. We hypothesize that a saturation of the normal-stress differences causes the sliding velocity to transition from a regime dictated by viscoelasticity, to a regime dictated by viscous lubrication. The exact details of the saturation of the normal stresses and the transition to lubrication require further analysis.

Spheres. – Having analyzed the dynamics of the sliding cylinder, we now extend our study to spheres. Using the same experimental set-up, we measure the speed and rotation of a steel sphere with radius $R = 0.5$ cm. Figure 4(a) shows the velocity U against the inclination angle α. We observe a strong phenomenological difference with respect to the cylinders, as the addition of polymers now decreases the sliding speed, regardless of the inclination angle (see the supplementary movie `SuppVid3.mp4`). At low inclination angles, the spheres also undergo strong stick-slip motion, for every polymer concentration. However, the stick-slip motion gradually disappears with increasing inclination angles, even for the Newtonian and weakly viscoelastic liquids. This result is also reflected in evolution of the relative rotation $\omega R/U$ against the inclination angle α (fig. 4(b)). At small inclination angles, the relative rotation is high for all liquids tested. However, the slip-free regime ($\omega R/U = 1$) is never observed and the spheres undergo stick-slip motion (see the supplementary

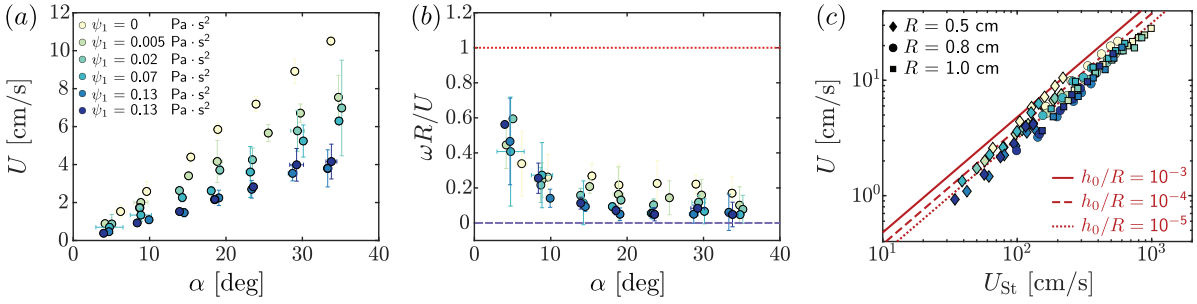

Fig. 4: (a) The velocity U for a sphere with radius $R = 0.5$ cm against the inclination angle α. Increasing the value of ψ_1 reduces the velocity. (b) The relative rotation speed $\omega R/U$ smoothly decreases with α, while viscoelasticity has a minor effect. (c) The experimental velocity U against the Stokes velocity U_{St} for different sphere sizes and polymer concentrations. The red lines correspond to the Newtonian lubrication theory, given by (7), for $h_0/R = 10^{-3}, 10^{-4}$, and 10^{-5}.

movie `SuppVid4.mp4`). Increasing the inclination angle leads to a smooth decrease of the relative rotation, which saturates to a small value near 0, for angles larger than 20° for each liquid.

The polymer concentration does not strongly affect the rotation, with smaller rotation occurring as ψ_1 increases. This observation is in qualitative agreement with a recent experimental study, which demonstrated that normal stresses did not affect the lubrication of spherical contacts [34]. The smooth transition towards low relative rotation suggests that the sphere gradually switches from a mixed lubrication regime to a hydrodynamic lubrication regime. This behavior is much different from the response observed for the cylinders, where the pure sliding regime was abruptly obtained (high viscoelasticity) or never reached (low viscoelasticity). Therefore, the flow geometry may play an important role on how the transition to the hydrodynamic lubrication regime is achieved.

We continue by testing the sphere velocities against the Stokes velocity scale U_{St}. We also include the data obtained for steel spheres with radii of $R = 0.8$ cm and $R = 1$ cm. While the Stokes velocity failed to capture the data for the cylinders (fig. 3(a)), the data for all three spheres collapse onto a straight line (fig. 4(c)). The Stokes velocity on the horizontal axis has a higher order of magnitude than the velocities observed in our experiments, which can be attributed to the effects of lubrication. A sphere moving parallel to a wall at a gap distance $h_0 \ll R$ experiences a horizontal viscous drag that has been shown to follow the asymptotic expression $\mathcal{D} = 6\pi\eta U R[0.95 + (8/15)\ln(R/h_0)]$ [35,36]. Balancing the viscous drag with the weight component $(4\pi/3)\Delta\rho g R^3 \sin\alpha$ yields a velocity prediction

$$U = U_{\mathrm{St}}\left[4.29 + \frac{12}{5}\ln\left(\frac{R}{h_0}\right)\right]^{-1}. \qquad (7)$$

The logarithmic term makes the dependence of U on h_0 weak. To test this prediction, we plot (7) using values of the ratio $h_0/R = 10^{-3}$, 10^{-4}, and 10^{-5}, which correspond to a film thickness in the range of 0.05 to 10 μm. The resulting curves have small differences and are in good agreement with the experimental data (red lines in fig. 4(c)). This agreement suggests that the decrease in velocity with ψ_1 is not due to normal-stress differences but the increase of the solution viscosity (see the SM). Therefore, we can conclude that normal-stress differences have a limited influence on the lubrication of the spherical contact.

Spherical and cylindrical contacts exhibit differences even in Newtonian lubrication. During the translation parallel to a wall, the flow induces a torque on the sphere but not on the cylinder. The effect of geometry also extends to viscoelastic lubrication, where normal-stress effects are absent in spheres but apparent in cylinders. For the two-dimensional flow below the cylinder, Tanner's theorem allows for a direct calculation of the viscoelastic stresses. However, this theorem does not apply for three-dimensional flows, and thus computing the viscoelastic stresses in spherical lubrication becomes non-trivial. The necessity of computing the viscoelastic stresses can be overcome via the reciprocal theorem, which directly yields the lift force, but does not provide any information on the actual stresses inside the contact region. This theoretical approach leads to an attractive force between a sphere and wall or between two spheres [17,37], which is consistent with experimental and numerical [18–21] observations. Yet, even if such normal stresses were present, it is unclear if their contribution is significant compared to viscous effects. The good agreement between the experimental data and Newtonian lubrication theory (fig. 4(c)), supports our claim that normal-stress differences have little influence in lubricated spherical contacts.

Conclusion and outlook. – To summarize, we have investigated the dynamics of cylinders and spheres moving down an inclined plane inside a viscoelastic liquid bath. Our experiments revealed that when submerged in highly viscoelastic liquids, cylinders adopt faster sliding speeds compared to Newtonian liquids. The stretching of the dissolved polymers induces a lift force and pushes the cylinder away from the wall, which promotes the transition towards hydrodynamic lubrication and leads to smaller sliding friction as compared to Newtonian liquids. We showed that the second-order fluid model leads

to an analytical expression for the lift, which can be used to obtain a prediction for the cylinder sliding velocity. The theoretical prediction captured well the observed sliding speed for relatively low inclination angles. At larger angles, the prediction overestimates the sliding velocity, which is likely due to the saturation of the normal stresses. Indeed, the second-order fluid model is strictly limited for steady and weakly viscoelastic flows. Therefore, invoking more complex constitutive relations, such as the Giesekus or FENE models, could provide a more accurate description of normal-stress effects. The polymers lead to an opposite effect for sliding spheres, whose velocity decreased with polymer concentration. The sliding speed was well described by Newtonian lubrication theory, suggesting that normal stresses have a minor influence on the sphere motion. Therefore, the extreme slipperiness that is often associated with polymer solutions relies on whether normal stresses generate an upward lift force. The normal stresses crucially depend on the flow geometry but also on the direction in which the object is moving. Indeed, viscoelastic lift forces also manifest in unsteady squeeze flows [38], where they significantly prolong the drainage of thin liquid films.

Our experimental findings open new perspectives in viscoelastic lubrication. A natural extension would be to measure the film thickness and the sliding friction for viscoelastic lubricants in the hydrodynamic regime [39]. Such experiments could elucidate how the thickness varies for the cases with large sliding velocities, and whether a transition from viscoelastic to viscous lubrication indeed exists. We expect our results to provide insight into the dynamics of particle suspensions in viscoelastic liquids [40,41], where polymer stretching complements the particle interactions to the resulting normal stresses.

* * *

We thank C. Datt and H. Stone for stimulating discussions and R. Zenit for useful insights on the preparation of Boger fluids. This work is supported by the N.W.O. through the VICI Grant No. 680-47-632.

Data availability statement: The data that support the findings of this study are available upon reasonable request from the authors.

REFERENCES

[1] Mow V. C. and Lai W., *Annu. Rev. Fluid Mech.*, **11** (1979) 247.
[2] Hamrock B. J. *et al.*, *Fundamentals of Fluid Film Lubrication* (CRC Press) 2004.
[3] Oron A. *et al.*, *Rev. Mod. Phys.*, **69** (1997) 931.
[4] Jeffrey D. and Onishi Y., *Q. J. Mech. Appl. Math.*, **34** (1981) 129.
[5] Sekimoto K. and Leibler L., *Europhys. Lett.*, **23** (1993) 113.
[6] Skotheim J. and Mahadevan L., *Phys. Rev. Lett.*, **92** (2004) 245509.
[7] Snoeijer J. H. *et al.*, *Phys. Fluids*, **25** (2013) 101705.
[8] Salez T. and Mahadevan L., *J. Fluid Mech.*, **779** (2015) 181.
[9] Rallabandi B. *et al.*, *Phys. Rev. Fluids*, **2** (2017) 074102.
[10] Zhang Z. *et al.*, *Phys. Rev. Lett.*, **124** (2020) 054502.
[11] Essink M. H. *et al.*, *J. Fluid Mech.*, **915** (2021) A49.
[12] Saintyves B. *et al.*, *Proc. Natl. Acad. Sci. U.S.A.*, **113** (2016) 5847.
[13] Morozov A. and Spagnolie S. E., in *Complex Fluids in Biological Systems: Experiment, Theory, and Computation* (Springer) 2015, p. 3.
[14] Joseph D. *et al.*, *J. Non-Newton. Fluid Mech.*, **54** (1994) 45.
[15] Binous H. and Phillips R. J., *J. Non-Newton. Fluid Mech.*, **83** (1999) 93.
[16] Ardekani A. *et al.*, *Phys. Fluids*, **20** (2008) 063101.
[17] Khair A. S. and Squires T. M., *Phys. Rev. Lett.*, **105** (2010) 156001.
[18] Liu Y. J. *et al.*, *J. Non-Newton. Fluid Mech.*, **50** (1993) 305.
[19] Becker L. *et al.*, *J. Non-Newton. Fluid Mech.*, **63** (1996) 201.
[20] Binous H. and Phillips R. J., *J. Non-Newton. Fluid Mech.*, **85** (1999) 63.
[21] Singh P. and Joseph D., *J. Non-Newton. Fluid Mech.*, **94** (2000) 179.
[22] Feng J. *et al.*, *J. Non-Newton. Fluid Mech.*, **63** (1996) 63.
[23] James D. F., *Annu. Rev. Fluid Mech.*, **41** (2009) 129.
[24] Keim N. C. *et al.*, *Phys. Fluids*, **24** (2012) 081703.
[25] Tanner R. I. and Dai S., *Rheol. Acta*, **55** (2016) 739.
[26] Castillo A. *et al.*, *Phys. Rev. Fluids*, **4** (2019) 063302.
[27] Su Y. *et al.*, *Phys. Rev. Fluids*, **6** (2021) 033303.
[28] Soetrisno D. D. *et al.*, *Macromolecules*, **56** (2023) 4919.
[29] Persson B. N., *Sliding Friction: Physical Principles and Applications* (Springer Science & Business Media) 2013.
[30] Veltkamp B. *et al.*, *Phys. Rev. Lett.*, **126** (2021) 044301.
[31] Bird R. B. *et al.*, *Dynamics of Polymeric Liquids*, Vol. **1**: *Fluid Mechanics* (John Wiley and Sons Inc., New York, NY) 1987.
[32] Tanner R. I., *Engineering Rheology*, Vol. **52** (Oxford University Press, Oxford) 2000.
[33] Oratis A. *et al.*, *Interfacial Flows – The Power and Beauty of Asymptotic Methods* (Springer) 2025, in print (`https://link.springer.com/book/9783031787638`).
[34] Veltkamp B. *et al.*, *Phys. Rev. Appl.*, **19** (2023) 014056.
[35] Goldman A. J. *et al.*, *Chem. Eng. Sci.*, **22** (1967) 637.
[36] O'neill M. and Stewartson K., *J. Fluid Mech.*, **27** (1967) 705.
[37] Dandekar R. and Ardekani A. M., *Phys. Fluids*, **33** (2021) 083112.
[38] Veltkamp B. *et al.*, *J. Fluid Mech.*, **951** (2022) A40.
[39] Dong H. *et al.*, *Adv. Mater.*, **35** (2023) 2211044.
[40] Koch D. L. and Subramanian G., *J. Non-Newton. Fluid Mech.*, **138** (2006) 87.
[41] Housiadas K. D. and Tanner R. I., *J. Non-Newton. Fluid Mech.*, **162** (2009) 88.